Realization of Subwavelength Asymmetric Acoustic Transmission Based on Low-Frequency Forbidden Transmission

Sai Zhang,[1] Yu Zhang,[1,2,*] Yijun Guo,[1] Yanhong Leng,[1] Wen Feng,[1] and Wenwu Cao[3,†]

[1]*Key Laboratory of Underwater Acoustic Communication and Marine Information Technology of the Ministry of Education, Xiamen University, Xiamen 361005, China*

[2]*State Key Laboratory of Marine Environmental Science, Xiamen University, Xiamen 361005, China*

[3]*Department of Mathematics and Materials Research Institute, The Pennsylvania State University, University Park, Pennsylvania 16802, USA*

(Received 15 May 2015; revised manuscript received 22 January 2016; published 10 March 2016)

Asymmetric transmission devices that allow acoustic waves to propagate only along one direction receive significant attention because of the rich physics and many potential applications. However, most proposed designs, such as acoustic superlattices and nonlinear acoustic diodes, are much larger than the wavelength, which are impractical for aqueous applications that require unidirectionality at low frequencies. In this work, subwavelength asymmetric acoustic transmission (SAAT) is realized based on low-frequency forbidden transmission of solid-fluid acoustic superlattices. Our design is comprised of a 1D superlattice serving as a low-frequency forbidden transmitter and a periodic rectangular grating serving as the wave-front converter. The SAAT structure and superlattice constant are only 0.6λ and 0.128λ, respectively, where λ is the wavelength, while a very high rectifying efficiency of over 10^8 is achieved. This SAAT design breaks the size-wavelength limitation to allow unidirectional low-frequency acoustic wave transmissions, which is desirable for the miniaturization of integrated acoustic devices in unidirectional signal-transmission applications.

DOI: 10.1103/PhysRevApplied.5.034006

I. INTRODUCTION

In the past several decades, inspired by the rectification capability of electronic diodes, considerable efforts have been devoted to asymmetric transmission of various forms of energy fluxes [1–18]. Optical diodes [15,16], thermal diodes [17,18], and acoustic diodes (ADs) [1–14] have been extensively investigated, and significant advances have been achieved in corresponding fields. Phononic crystals and acoustic metamaterials have been found to play a role in the fabrication of asymmetric acoustic transmission devices and have been applied in a variety of energy manipulations, such as negative refraction [19,20], directive emission [21,22], and other extraordinary transmissions [23,24].

For practical applications, miniaturization and low-energy consumption are the inevitable developing trend of acoustic devices. Recently, a highly nonlinear metamaterial-based AD with subwavelength size proposed by Popa and Cummer [1] has achieved nonreciprocal transmission at audio frequencies. Another compact acoustic nonreciprocal device called an acoustic circulator for airborne sound waves inspired by the electromagnetic nonreciprocity in magneto-optical media was presented by Alù and co-workers [2]. In their designs, the one-way response of the subwavelength nonreciprocal transmission devices needs to have external power supplies; hence, they are called active asymmetric transmission systems. Differing from these schemes, some passive asymmetric transmission designs based on phononic crystals have been proposed for convenience of application and energy savings [3–6]. Usually, in these designs, the nonlinearity was introduced to break time-reversal symmetry. For example, Liang *et al.* [3,4] performed theoretical and experimental studies on an AD comprised of a superlattice (SL) with a strong nonlinear medium. One-way response is attributed to the principle that the fundamental and second harmonic waves are in the stop band and passband of the SL, respectively. In order to preserve the frequencies of the energy flux and obtain high forward transmission, Liu and co-workers [6] have presented an AD model consisting of a weakly nonlinear phononic crystal with asymmetric linear structures at the two ends of the proposed structure. In addition to the nonlinear mechanisms, pure linear designs have been proposed to realize unidirectional transmission by introducing diffraction structures to break the spatial reversal symmetry [7–13], although such designs are reciprocal asymmetric systems and should not be called diodes [14]. For instance, Li *et al.* [7] have constructed a phononic-crystal-based AD by using mode transitions at the opposite sides of the diode. Zhang and Zhang [13] proposed a broadband asymmetric transmission device by using acoustic metamaterials as a gradient-index structure. However, all existing phononic-crystal-based acoustic asymmetric

*Corresponding author.
yuzhang@xmu.edu.cn
†Corresponding author.
dzk@psu.edu

transmissions have the fundamental size-wavelength limitation [3–6,7,11]; i.e., the device size L must be sufficiently larger than the acoustic wavelength (λ) to allow multiple scattering, which cannot be realized for subwavelength-size ($L < \lambda$) devices. This is because these devices are based on the band-gap phenomenon when acoustic waves propagate within a period; thus, one-way subwavelength transmission cannot be achieved using this principle. For device miniaturization, it is desirable to have asymmetric transmission structures with compact and subwavelength size, which requires the design to overcome this size-wavelength limitation. Of course, a practical subwavelength asymmetric acoustic transmission (SAAT) must also have high rectifying efficiency.

In this paper, we propose a design of a SAAT device ($L < \lambda$) by coupling a 1D solid-fluid SL with a rectangular grating of periodically arranged rigid bars having its periodic direction perpendicular to that of the superlattice. The whole assembly is immersed in a water tank. Subwavelength unidirectivity is realized due to the low-frequency forbidden transmission of the solid-fluid SL. This passive SAAT device does not need external active power and achieves extremely high rectifying efficiency. The rectifying mechanism of the SAAT is carefully analyzed theoretically. Full-wave simulations are performed to derive the transmission ratios over a broadband of frequencies. Gauss-beam simulations are also performed to reveal the capability of the SAAT device for one-way propagation of an acoustic beam with spatially nonuniform wave-front intensity. Finally, the performance of the proposed SAAT model is verified experimentally, and the measured results qualitatively agree with the numerical predictions.

II. THEORY AND NUMERICAL SIMULATIONS

A. System design

As schematically shown in Fig. 1(a), the proposed SAAT design consists of two parts. The first part is an N layer ($N = 4$ here) 1D SL made of solid material I (PMMA) and fluid material II (water). The second part is a 1D periodically arranged rigid bar made of material III (steel) immersed in water. The structural parameters of the unit cell in Fig. 1(b) are $d_0 = 1$ mm, $d_{\rm I} = 2$ mm, $d_{\rm II} = 1$ mm, $d_{\rm III} = 2$ mm, $a = 10$ mm, and $A = 16$ mm. Thus, the total length L of our model structure is 14 mm, and the lattice constant D of the main superlattice is 3 mm. The forward incidence (FI) and backward incidence (BI) directions are indicated by arrows in Fig. 1(a). The whole three-dimensional structure is illustrated in Fig. 1(c). In this work, the omnidirectional transmission of the solid-fluid superlattice is computed through the transfer-matrix method [25,26], whereas the asymmetric transmission device operation is demonstrated through stationary simulations using the finite-element package COMSOL MULTIPHYSICS. In the simulations, the material parameters are adopted as follows:

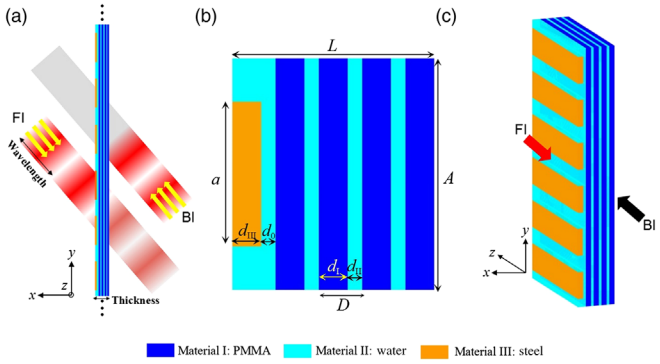

FIG. 1. (a) The schematic illustration of the SAAT device. The FI and BI are indicated by arrows. The wavelength of the incident acoustic wave is much larger than the thickness of the structure. (b) Schematic presentation of a unit cell of the SAAT structure. (c) Three-dimensional illustration of the SAAT structure.

mass density $\rho_{\rm I} = 1180$ kg/m^3, longitudinal wave velocity $c_{Il} = 2700$ m/s, transversal wave velocity $c_{It} = 1300$ m/s for PMMA plates, $\rho_{\rm II} = 1000$ kg/m^3, $c_{\rm IIl} = 1500$ m/s for water, and $\rho_{\rm III} = 7800$ kg/m^3, $c_{\rm IIIl} = 6100$ m/s, and $c_{\rm IIIt} = 3300$ m/s for steel.

B. Realization of subwavelength asymmetric transmission of acoustic energy flux

1. Low-frequency forbidden transmission of solid-fluid superlattice

The subwavelength transmission characteristics of the four-layer solid-fluid SL is shown in Fig. 2, where the transmission coefficient is calculated using the transfer-matrix method [25] as a function of both frequency and incident angle to the SL. Low-frequency forbidden transmission represents a rapid energy attenuation when the lattice constant becomes much less than the wavelength, which is different from the band gaps (see the first Bragg band gap in Fig. 2) induced due to Bragg scattering. Figure 3 shows the transmission coefficients of a PMMA-water SL with different

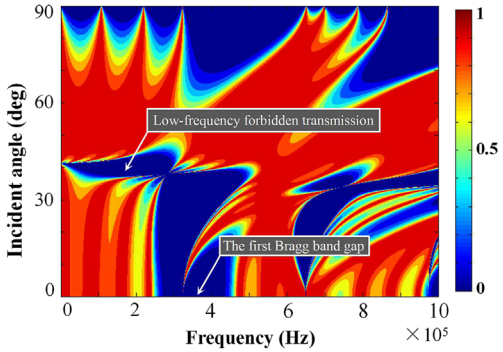

FIG. 2. Transmission coefficient as a function of frequency and incident angle of the four-layered PMMA-water SL. Low-frequency forbidden transmission is indicated by the arrow. For reference, the first Bragg band gap of the superlattice for normal incidence is also shown.

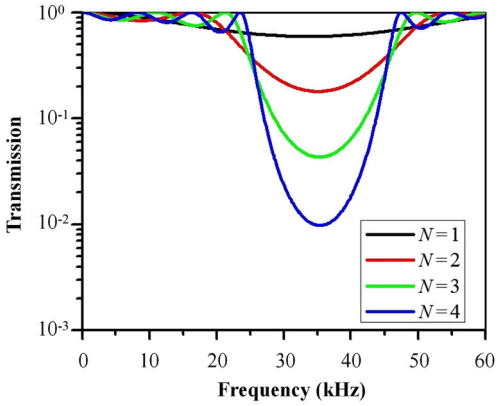

FIG. 3. Transmission coefficients of the PMMA-water SL with layer number $N = 1$, 2, 3, and 4 when the incident angle is at 0°.

layer number N when the incident angle is at 0°. We can see that with the increase of N, the first Bragg band gap gradually forms at the frequency of 350 kHz. The corresponding transmission coefficient of a four-layer SL is about 10^{-2}. However, for the low-frequency forbidden transmission shown in Fig. 2, a low transmission coefficient of less than 10^{-5} at 67.5 kHz is obtained for a single layer when the incident angle is at 41°, as shown in Fig. 4. When N increases to 4, we can obtain a transmission coefficient less than 10^{-20}. It is worth noting that the transmission coefficient of the SL with $N > 1$ at 67.5 kHz coincides exactly with the transmission coefficient of one solid PMMA plate inserted in water. This significant transmission difference between the low-frequency forbidden transmission and the first Bragg band gap suggests that the former can serve as a good candidate to fabricate subwavelength asymmetric acoustic transmission.

A comprehensive theoretical analysis of acoustic wave propagation in finite solid-fluid SLs with omnidirectional incidence has been investigated by the Green's function method [27,28]. It is shown that the band gaps of SLs stem from not only the periodicity of the system (Bragg-type gaps) but also the transmission zeros caused by the presence of the solid layers immersed in the fluid [27]. Here, the low-frequency forbidden transmission is attributed to the transmission zeros, which are at lower frequency compared to the first Bragg band gap.

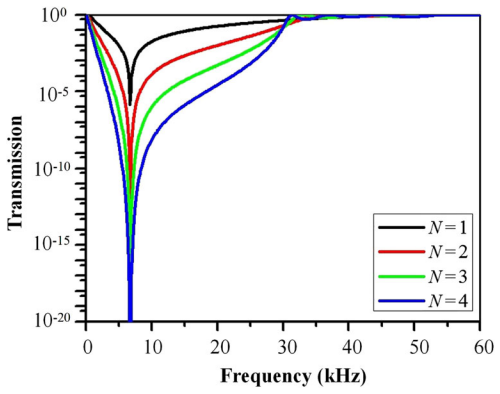

FIG. 4. Transmission coefficients of the PMMA-water SL with layer number $N = 1$, 2, 3, and 4 when the incident angle is fixed at 41°.

To gain deeper insight into the influence of fluid on the low-frequency forbidden transmission, let us consider a single unit of the SL. The transmission characteristic of an obliquely incident longitudinal wave through a solid plate immersed in fluid reveals an interesting phenomenon: with the increase of the ratio of fluid to solid density, the phase velocity curve of the Lamb wave deviates strongly from the S_0 mode at low frequencies [29]. In particular, when the fluid density is closed to that of the solid plate, the S_0-mode Lamb wave will not propagate in the low-frequency range, revealing a low-frequency forbidden transmission phenomenon. With the increase of the number of superlattice units, low-frequency forbidden transmission will be further enhanced due to the multiple scattering of the S_0-mode waves. However, for other incident angles, the superlattice has high transmission since other Lamb wave modes will not be evanescent, as shown in Fig. 2. In addition, our recent research results reveal that broader incident angles of low-frequency forbidden transmission at the subwavelength scale ascribe to the specific relationship among the three sound velocities: $c_{\mathrm{I}l} < c_{\mathrm{II}l} < c_{\mathrm{I}l}$ [30]. Thus, the Bragg scattering of the superlattice might not be the mechanism of the low-frequency forbidden transmission at 41°.

2. Simulation results

The low-frequency forbidden transmission property of the solid-fluid SL may be used to control acoustic energy flow in the SAAT structure. For the BI of a plane wave with an incidence angle of 41°, the transmission is forbidden. Conversely, for the FI, we use an acoustic grating of periodically arrayed rectangular bars to distort the wave front before it enters the main superlattice. High transmission appears when the incident angles of diffracted waves deviate from 41° caused by the grating. As a result, the SAAT structure leads to a one-way subwavelength response. To demonstrate this, full-wave simulations are implemented to evaluate the transmission property of the SAAT structure, as shown in Fig. 5. For the simulation, the structure considered consists of three primitive cells, which are immersed in water, and the periodic boundary condition is imposed on the top and bottom boundaries.

Figure 5 shows the acoustic pressure distribution of fluid and the displacement distribution of the solid of the SAAT structure. The plane wave with the frequency of 65 kHz ($\lambda \approx 1.65L$) is incident at an angle of 41° to the normal direction for both the FI and BI transmissions. The transmission coefficients of the FI and BI waves are denoted by T_F and T_B, respectively. In the case of BI, the incident subwavelength wave cannot transmit through the superlattice,

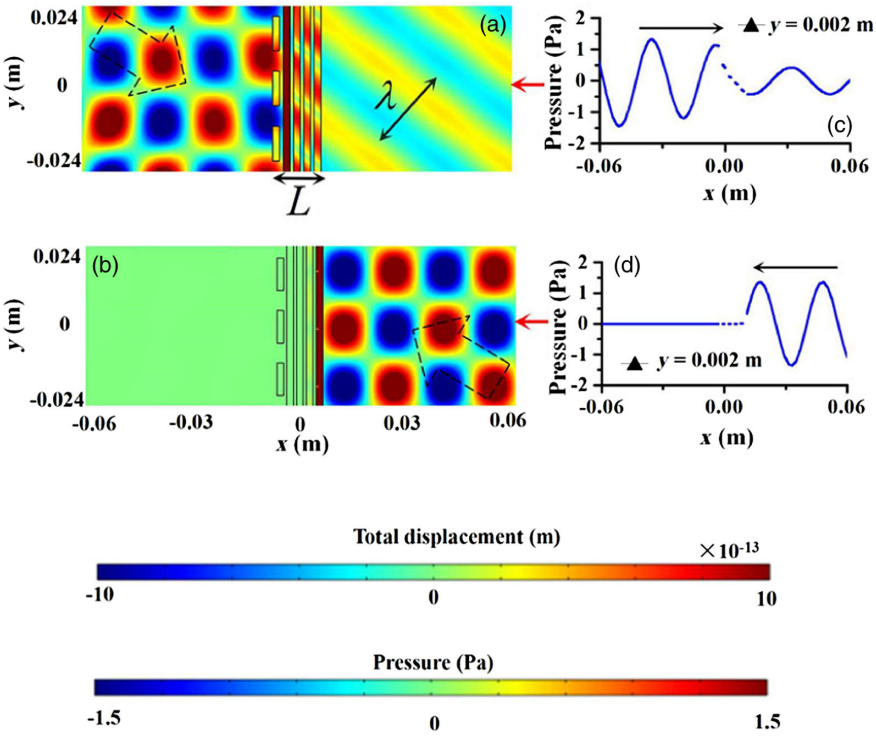

FIG. 5 (a),(b) Simulated acoustic pressure and displacement distributions for the BI and FI cases at the frequency of 65 kHz. Dashed black hollow arrows indicate the propagation directions. (c),(d) show the pressure distributions at $y = 0.002$ m.

leading to $T_B = 7.1 \times 10^{-9}$. Thus, there are no significant waves passing through the SAAT structure [Fig. 5(b)]. The forbidden transmission at 41° in the BI case agrees well with the above theoretical prediction in Fig. 2. However, in the case of FI, the transmitted wave with an amplitude as high as 50% of the incident wave and $T_F = 0.43$ are obtained, as shown in Fig. 5(a), where the wavelength λ is much larger than the total thickness L. It is noteworthy to point out that the waves on the incident side form some regular dots instead of a plane-wave pattern due to the interference between the incident and reflection waves. Figures 5(c) and 5(d) illustrate the pressure distributions of the two cases at $y = 0.002$ m. High forward transmission to the right side of Fig. 5(c) stands in sharp contrast to that of Fig. 5(d), where almost no waves pass through in the backward transmission.

Figure 6(a) shows the transmission coefficient of the waves transmitting to the right and left sides (corresponding to FI and BI, respectively) as a function of frequency. The transmission of the SAAT structure exhibits one-way response in a broad frequency range (see the gray shaded area). The transmission ratio T_F/T_B as high as 10^8 is obtained even when the total scale of the SAAT structure and the lattice constant are only 0.6λ and 0.128λ, respectively. It should be pointed out that the incident angle, which produces the transmission zero of SL, is frequency dependent although it changes slightly with the increase of frequency at low frequencies (see Fig. 2). Therefore, this SAAT structure can attain subwavelength asymmetric transmission not only at 41° but in a relatively wide range of angles from 37° to 42°. A comparison of the transmission ratio $\zeta = [(T_F - T_B)/(T_F + T_B)]$ of our SAAT structure with other reported asymmetric transmission results [1,3,9–12] as a function of L/λ is shown in Fig. 6(b). $L/\lambda = 1$ is the upper limit of the subwavelength range and $\zeta > 0.8$ is considered high rectifying performance.

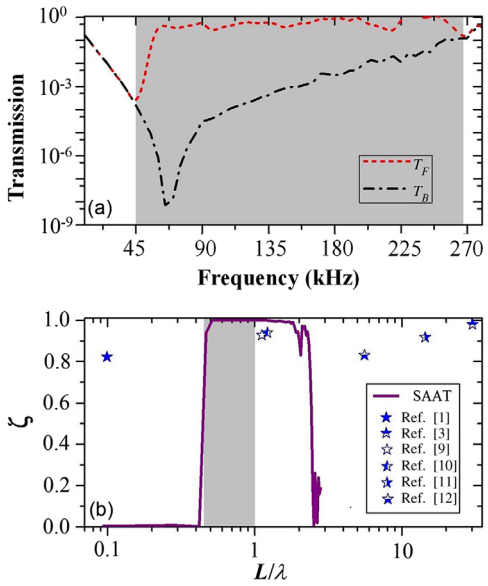

FIG. 6. (a) Transmission spectra of the SAAT structure for waves transmitting to the right and left (FI and BI, respectively) of the structure as a function of frequency. The gray shaded area shows the range of effective rectification. (b) Comparison of transmission contrast ratio ζ of our SAAT structure as a function of L/λ with asymmetric devices reported in Refs. [1, 3, 9–12]. The shaded region denotes the subwavelength range of rectification.

Within the subwavelength regime of $0.467 < L/\lambda < 1$ (see the shaded region), our SAAT structure shows highly efficient rectification. In the higher-frequency range ($1 < L/\lambda < 2.3$), high ζ is also found, indicating that the SAAT is also applicable as an effective asymmetric transmission device. Based on our calculations, ζ remains greater than 0.8 in the range of $0.467 < L/\lambda < 2.3$. In Refs. [3,9–12], their devices had high ζ, but their sizes did not satisfy the subwavelength requirement (see the blue stars). In Ref. [1], the asymmetric transmission device has a size as low as 0.1λ, but it is an audio system instead of an underwater device, and most important, it is an active device requiring additional energy consumption, and the rectifying performance is not efficient. Compared with all previously reported asymmetric transmission schemes, our SAAT design has the advantages of subwavelength size with high rectifying efficiency in a broader frequency range and does not need external power.

Furthermore, our SAAT structure is also applicable for unidirectional transmission of an acoustic beam with nonuniform wave-front intensity. Figure 7 shows the acoustic field distributions for the FI and BI of an acoustic beam, where the incident wave is a spatial Gaussian beam with the beam width of 37.2λ at 93 kHz. In the simulation, the total length in the x direction and y direction is 3.6 and 4.5 m, respectively. Perfectly matched layers are imposed on the top and bottom boundaries and the corresponding output side. For the FI case, two beams with different propagation directions appear on the right side of the structure due to the scattering from the acoustic grating; however, there are almost no waves on the left side of the SAAT structure for the BI case.

3. Experimental results

To verify the existence of low-frequency forbidden transmission of the SL and the performance of the SAAT in the experiment, we measure the acoustic power transmissions by the well-known ultrasonic transmission technique [31,32]. In the experiment, the prototype of the SAAT is realized according to the structure shown in Fig. 1, by coupling a four-layer 1D PMMA-water superlattice with 1D periodically arranged rigid steel bars. The sizes of the prototypes in the y and z directions are 600 and 400 cm, respectively, and the structural parameters of the unit cells are the same as those used in Fig. 1. Figure 8(a) shows the schematic diagram of the experiment, where the entire assembly is immersed in a $1.5 \times 1 \times 1$ m^3 water tank, and

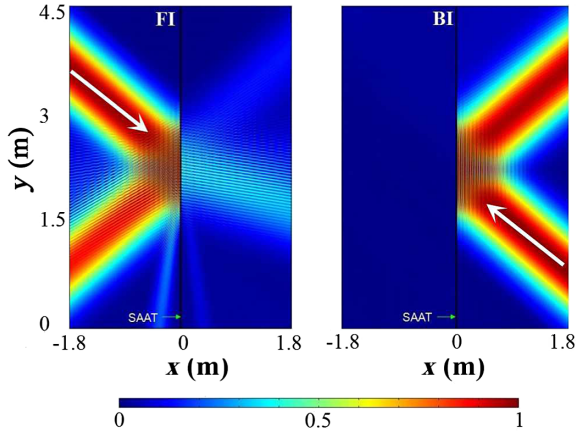

FIG. 7. Propagations of a Gaussian beam through the SAAT structure for FI (left) and BI (right) cases. White arrows indicate the wave propagation directions.

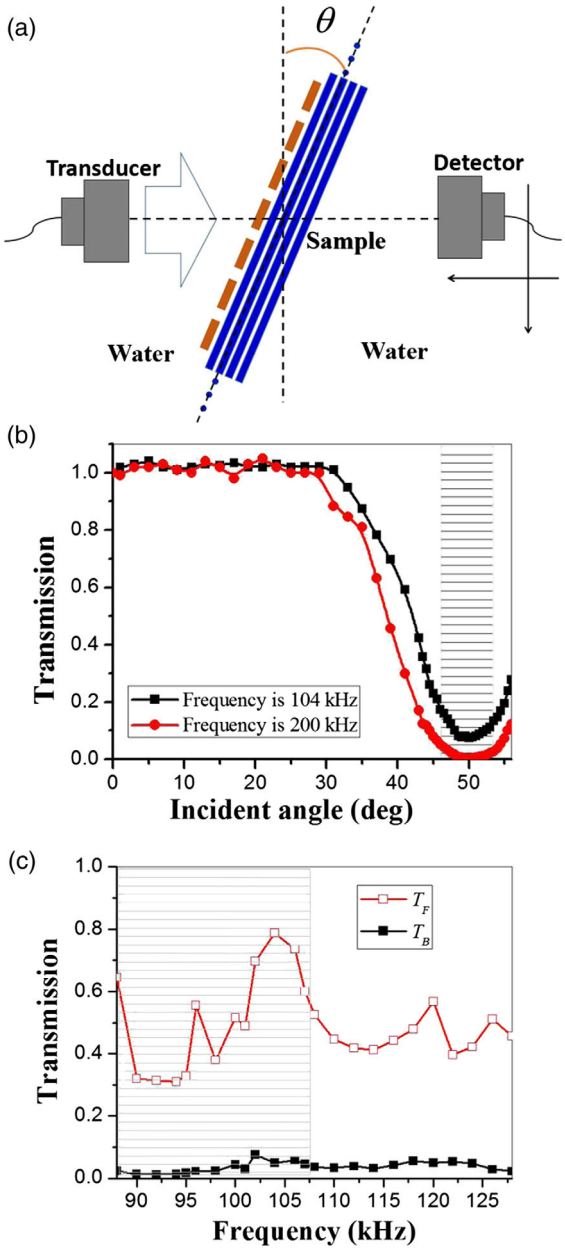

FIG. 8. (a) Schematic diagram of experimental setup. (b) Experimentally measured transmission spectra at 104 and 200 kHz as a function of the incident angle for a four-layer PMMA-water SL. (c) Experimental transmission spectra of SAAT as a function of frequency for FI and BI.

the water temperature is 297 K. The SL or SAAT is clamped and placed between a pair of specially designed ultrasonic generation and detection transducers (with the central frequencies of 200 kHz and bandwidths of 100–300 kHz). The angle θ is controlled by a high-precision rotary device.

Figure 8(b) shows the experimental acoustic power transmission spectra as a function of incident angle θ at two given frequencies 200 and 104 kHz. It is apparent that the incident angle of the low-frequency forbidden transmission occurs at 50° (as shown in the shaded area), which is a little bigger than the theoretical prediction. Besides, the transmission value of 200 kHz at 50° is much smaller than that of 104 kHz and is sufficiently close to zero, as the transducer has a better directivity at center frequency. Figure 8(c) shows the measured transmittance spectra of the waves transmitting to the right when $\theta = 50°$ and 230° (corresponding to the FI and BI, respectively) as a function of frequency. Obviously, the transmission of the SAAT sample exhibits a one-way response in a broad frequency range from 88 to 128 kHz, which agrees well with the numerical results in Fig. 6(a). Some practical factors, such as the directivity of the transducer and the structural parameters, affect the measured accuracy of the above experimental results, which should be further investigated.

III. SUMMARY AND CONCLUSIONS

In summary, we design an efficient SAAT structure by assembling a 1D solid-fluid SL stacking with a rectangular acoustic grating, in which unidirectional transmission of underwater acoustic waves can be realized in the subwavelength regime. In our design, a special low-frequency forbidden transmission of a solid-fluid SL at oblique incidence is utilized to block the backward incident waves, which not only has a more powerful blocking performance but also works at lower operating frequency, in contrast to the first Bragg band-gap principle used in previous designs [2–4]. With this design, we achieve several improvements and outstanding features: First, our design realizes a very high transmission ratio within the subwavelength regime, which breaks the size-wavelength limit for one-way acoustic wave transmission. Second, our design keeps the waveform consistent between the input and output waves [see Fig. 3(a)] and avoids excessive energy divergence induced by the interference of numerous outgoing beams from different diffraction orders because our SAAT structure works in a relatively low-frequency range. Compared with other subwavelength asymmetric transmission models in the literature [1,2], our SAAT structure can achieve high-efficiency one-way response without any acoustic nonlinearity. As with other linear ADs, our SAAT structure inevitably obeys the acoustic reciprocity principle [14]. However, if we combine the excellent reverse blocking property of low-frequency forbidden transmission with nonlinearity like the AD design proposed by Liang *et al.* [3,4], a compact nonreciprocal structure may be realized.

This SAAT design realizes nearly perfect transmission ratio within the subwavelength region $0.467 < L/\lambda < 1$, which breaks the size-wavelength limit for one-way acoustic wave transmission, and it also has a very broad working band with ζ remaining greater than 0.8 in the range of $0.467 < L/\lambda < 2.3$. Compared to previously reported asymmetric transmission schemes, our design does not need external power and is superior in the subwavelength regime with much broader bandwidth. All these characteristics are beneficial for the miniaturization of integrated acoustic devices in unidirectional signal-transmission applications.

ACKNOWLEDGMENTS

This work is supported in part by the National Science Foundation of China (Grants No. 41276040 and No. 11174240) and the Natural Science Foundation of Fujian Province of China (Grant No. 2012J06010). The project is sponsored by the Scientific Research Foundation for the Returned Overseas Chinese Scholars, State Education Ministry. We thank Professor Yan Li for his suggestions in the early stage of this work.

[1] B. I. Popa and S. A. Cummer, Non-reciprocal and highly nonlinear active acoustic metamaterials, Nat. Commun. **5**, 3398 (2014).
[2] R. Fleury, D. L. Sounas, C. F. Sieck, M. R. Haberman, and A. Alù, Sound isolation and giant linear nonreciprocity in a compact acoustic circulator, Science **343**, 516 (2014).
[3] B. Liang, B. Yuan, and J. C. Cheng, Acoustic Diode: Rectification of Acoustic Energy Flux in One-Dimensional Systems, Phys. Rev. Lett. **103**, 104301 (2009).
[4] B. Liang, X. S. Guo, J. Tu, D. Zhang, and J. C. Cheng, An acoustic rectifier, Nat. Mater. **9**, 989 (2010).
[5] N. Boechler, G. Theocharis, and C. Daraio, Bifurcation based acoustic switching and rectification, Nat. Mater. **10**, 665 (2011).
[6] C. Liu, Z. Du, Z. Sun, H. Gao, and X. Guo, Frequency-Preserved Acoustic Diode Model with High Forward-Power-Transmission Rate, Phys. Rev. Applied **3**, 064014 (2015).
[7] X. F. Li, X. Ni, L. Feng, M. H. Lu, C. He, and Y. F. Chen, Tunable Unidirectional Sound Propagation through a Sonic-Crystal-Based Acoustic Diode, Phys. Rev. Lett. **106**, 084301 (2011).
[8] H. X. Sun, S. Y. Zhang, and X. J. Shui, A tunable acoustic diode made by a metal plate with periodical structure, Appl. Phys. Lett. **100**, 103507 (2012).
[9] Y. Li, J. Tu, B. Liang, X. S. Guo, D. Zhang, and J. C. Cheng, Unidirectional acoustic transmission based on source pattern reconstruction, J. Appl. Phys. **112**, 064504 (2012).
[10] H. Jia, M. Z. Ke, C. H. Li, C. Y. Qiu, and Z. Y. Liu, Unidirectional transmission of acoustic waves based on

asymmetric excitation of Lamb waves, Appl. Phys. Lett. **102**, 153508 (2013).
[11] S. Xu, C. Qiu, and Z. Liu, Acoustic transmission through asymmetric grating structures made of cylinders, J. Appl. Phys. **111**, 094505 (2012).
[12] R. Q. Li, B. Liang, Y. Li, W. W. Kan, X. Y. Zhou, and J. C. Cheng, Broadband asymmetric acoustic transmission in a gradient-index structure, Appl. Phys. Lett. **101**, 263502 (2012).
[13] S. Zhang and Y. Zhang, Broadband unidirectional acoustic transmission based on piecewise linear acoustic metamaterials, Chin. Sci. Bull. **59**, 3239 (2014).
[14] A. A. Maznev, A. G. Every, and O. B. Wright, Reciprocity in reflection and transmission: What is a "phonon diode"?, Wave Motion **50**, 776 (2013).
[15] F. D. M. Haldane and S. Raghu, Possible Realization of Directional Optical Waveguides in Photonic Crystals with Broken Time-Reversal Symmetry, Phys. Rev. Lett. **100**, 013904 (2008).
[16] D. W. Wang, H. T. Zhou, M. J. Guo, J. X. Zhang, J. Evers, and S. Y. Zhu, Optical Diode Made from a Moving Photonic Crystal, Phys. Rev. Lett. **110**, 093901 (2013).
[17] B. Li, L. Wang, and G. Casati, Thermal Diode: Rectification of Heat Flux, Phys. Rev. Lett. **93**, 184301 (2004).
[18] C. W. Chang, D. Okawa, A. Majumdar, and A. Zettl, Solid-state thermal rectifier, Science **314**, 1121 (2006).
[19] J. B. Pendry, Negative Refraction Makes a Perfect Lens, Phys. Rev. Lett. **85**, 3966 (2000).
[20] M. H. Lu, C. Zhang, L. Feng, J. Zhao, Y. F. Chen, Y. W. Mao, J. Zi, Y. Y. Zhu, S. N. Zhu, and N. B. Ming, Negative birefraction of acoustic waves in a sonic crystal, Nat. Mater. **6**, 744 (2007).
[21] L. Quan, X. Zhong, X. Z. Liu, X. F. Gong, and P. A. Johnson, Effective impedance boundary optimization and its contribution to dipole radiation and radiation pattern control, Nat. Commun. **5**, 3188 (2014).
[22] Y. Zhang, X. W. Gao, S. Zhang, W. W. Cao, L. G. Tang, D. Wang, and Y. Li, A biomimetic projector with high subwavelength directivity based on dolphin biosonar, Appl. Phys. Lett. **105**, 123502 (2014).
[23] J. Christensen, L. Martin-Moreno, and F. J. Garcia-Vidal, Theory of Resonant Acoustic Transmission through Subwavelength Apertures, Phys. Rev. Lett. **101**, 014301 (2008).
[24] Z. Liang and J. Li, Extreme Acoustic Metamaterial by Coiling Up Space, Phys. Rev. Lett. **108**, 114301 (2012).
[25] S. Zhang, Y. Zhang, and X. Gao, Superwide-angle acoustic propagations above the critical angles of the Snell law in liquid solid superlattice, Chin. Phys. B **23**, 124301 (2014).
[26] Y. Zhang, Y. Li, H. Shao, Y. Z. Zhong, S. Zhang, and Z. X. Zhao, Band gaps and localization of surface water waves over large-scale sand waves with random fluctuations, Phys. Rev. E **85**, 066319 (2012).
[27] Y. E. Hassouani, E. H. E. Boudouti, B. Djafari-Rouhani, and H. Aynaou, Sagittal acoustic waves in finite solid-fluid superlattices: Band-gap structure, surface and confined modes, and omnidirectional reflection and selective transmission, Phys. Rev. B **78**, 174306 (2008).
[28] E. H. E. Boudouti, B. Djafari-Rouhani, A. Akjouj, and L. Dobrzynski, Acoustic waves in solid and fluid layered materials, Surf. Sci. Rep. **64**, 471 (2009).
[29] A. H. Nayfeh and D. E. Chimenti, Propagation of guided waves in fluid-coupled plates of fiber-reinforced composite, J. Acoust. Soc. Am. **83**, 1736 (1988).
[30] S. Zhang, Y. Zhang, and X. Gao, Comparative study on the omnidirectional transmission characteristics of two types one-dimensional liquid-solid phononic crystals, J. Synth. Cryst. **43**, 9 (2014).
[31] B. Hou, J. Mei, M. Z. Ke, Z. Y. Liu, J. Shi, and W. J. Wen, J. Appl. Phys. **104**, 014909 (2008).
[32] H. Estrada, P. Candelas, A. Uris, and F. Belmar, F. J. Garcia de Abajo, and F. Meseguer, Appl. Phys. Lett. **95**, 051906 (2009).